ISSN 1674-1056
http://cpb.iphy.ac.cn
http://iopscience.iop.org/cpb
中国物理 B
Chinese Physics
中国物理 Chinese Physics B

In-situ growth of different numbers of gold nanoparticles on MoS_2 with enhanced electrocatalytic activity for hydrogen evolution reaction

Xuan Zhao(赵宣), Da-Wei He(何大伟), Yong-Sheng Wang(王永生), Chen Fu(付晨)
Citation: Chin. Phys. B . 2018, 27(6): 068103. **doi:** 10.1088/1674-1056/27/6/068103

Journal homepage: http://cpb.iphy.ac.cn; http://iopscience.iop.org/cpb

What follows is a list of articles you may be interested in

Nucleation mechanism and morphology evolution of MoS_2 flakes grown by chemical vapor deposition

He-Ju Xu(许贺菊), Jian-Song Mi(米建松), Yun Li(李云), Bin Zhang(张彬), Ri-Dong Cong(丛日东), Guang-Sheng Fu(傅广生), Wei Yu(于威)
Chin. Phys. B . 2017, 26(12): 128102. **doi:** 10.1088/1674-1056/26/12/128102

Synthesis of ZnO quantum dots and their agglomeration mechanisms along with emission spectra based on ageing time and temperature

Bo Qiao(乔泊), Suling Zhao(赵谡玲), Zheng Xu(徐征), Xurong Xu(徐叙瑢)
Chin. Phys. B . 2016, 25(9): 098102. **doi:** 10.1088/1674-1056/25/9/098102

Influences of hydrogen dilution on microstructure and optical absorption characteristics of nc-SiO_x:H film

Zhao Wei, Du Lin-Yuan, Jiang Zhao-Yi, Yin Chen-Chen, Yu Wei, Fu Guang-Sheng
Chin. Phys. B . 2015, 24(10): 108102. **doi:** 10.1088/1674-1056/24/10/108102

Improved performance of microcrystalline silicon solar cell with graded-band-gap silicon oxide buffer layer

Shi Zhen-Liang, Ji Yun, Yu Wei, Yang Yan-Bin, Cong Ri-Dong, Chen Ying-Juan, Li Xiao-Wei, Fu Guang-Sheng
Chin. Phys. B . 2015, 24(7): 078105. **doi:** 10.1088/1674-1056/24/7/078105

Influence of substrate bias voltage on the microstructure of nc-SiO_x:H film

Li Hui-Min, Yu Wei, Xu Yan-Mei, Ji Yun, Jiang Zhao-Yi, Wang Xin-Zhan, Li Xiao-Wei, Fu Guang-Sheng
Chin. Phys. B . 2015, 24(2): 028102. **doi:** 10.1088/1674-1056/24/2/028102

In situ growth of different numbers of gold nanoparticles on MoS_2 with enhanced electrocatalytic activity for hydrogen evolution reaction*

Xuan Zhao(赵宣)†, Da-Wei He(何大伟)‡, Yong-Sheng Wang(王永生)§, and Chen Fu(付晨)

Key Laboratory of Luminescence and Optical Information, Beijing Jiaotong University, Beijing 100044, *China*

(Received 26 October 2017; revised manuscript received 13 March 2018; published online 10 May 2018)

Producing hydrogen through a hydrogen evolution reaction (HER) by splitting water at the suitable overpotential is a great alternative to solving the problems of environmental pollution and the energy crisis. Molybdenum sulfide (MoS_2) has attracted extensive attention as one of the most promising catalytic materials for HER. In this work, we design a facile method to *in situ* grow gold nanoparticles (AuNPs) on MoS_2. Different numbers of AuNPs with $MoS_2$are used to find the best catalytic activity. Due to the larger active surface area and higher conductivity of the Au–MoS_2 composites, all the Au–MoS_2 composites exhibit more enhanced HER electroactivity than pure MoS_2. In brief, the new material architecture exhibits optimized HER activity with a low onset overpotential of 0.12 V, low Tafel slope of 0.163 V·dec^{-1}, and an excellent stability in acidic solution.

Keywords: MoS_2, AuNPs, hydrogen evolution reaction, electrocatalysts

PACS: 81.07.Bc, 81.10.Dn, 81.16.Dn, 82.30.Rs **DOI:** 10.1088/1674-1056/27/6/068103

1. Introduction

In recent years, the serious rapidly increasing energy crisis and the associated environmental pollution have promoted the development of renewable and clean alternative energy sources.[1–3] Due to the high energy density and zero carbon emission, hydrogen has attracted attention for replacing traditional fossil fuels and been considered as a promising next-generation clean fuel resource.[4–7] Electrochemically splitting water via hydrogen evolution reaction (HER) is an attractive way to produce hydrogen and regarded as an excellent energy carrier in the future.[8–10] To date, platinum (Pt) or its alloys is considered to be one of the most effective electrocatalysts for hydrogen evolution reaction,[11–13] however their high price and extreme shortage seriously hinder their broad-scale industrial applications.[14–16] Replacing Pt with highly effective catalysts based on earth-abundant elements is a challenging research problem.[17]

Due to a similar Gibbs free energy for hydrogen adsorption of platinum,[18–20] low cost and high abundance, molybdenum disulfide (MoS_2)-based electrocatalysts have attracted increasing attention.[21–25] Much work has been performed with the aim of improving the exposure of active sites of MoS_2 and facilitating the electron transportation in the HER process.[26–29] For example, by using density functional theory (DFT), Hinnemann *et al.* demonstrated that the basal plane of MoS_2 is catalytically inactive, however the edge sites are catalytically active for hydrogen evolution reaction.[30] Jaramillo *et al.* proved that the hydrogen evolution reaction activity of MoS_2 is proportional to the length of edge rather than the coverage area.[31] Smith *et al.* synthesized MoS_x grown on crumpled-graphene–modified carbon cloth composite catalyst, and significantly enhanced the hydrogen evolution reaction activity.[32] Huang *et al.* demonstrated that Pt–MoS_2 hybrid nanomaterials exhibit much higher electrocatalytic activity towards the hydrogen evolution reaction than the commercial Pt catalysts with the same Pt loading.[33]

In this work, we synthesize an Au–MoS_2 composite through *in situ* growth method. Gold nanoparticles (AuNPs) have various unique properties such as excellent conducting capability, high specific surface area and superior catalytic property.[34–37] The involvement of AuNPs can not only enhance the electronic property of MoS_2, but also increase the specific surface area of the composite. To improve the electrocatalytic performances of the Au–MoS_2 composites, different numbers of AuNPs with MoS_2 are evaluated by using a three-electrode system. All the composites exhibit significant enhancement in catalytic activity compared with pure MoS_2. To the best of our knowledge, this is the first report on synthesizing AuNPs for the MoS_2 and utilizing the composite for catalyzing hydrogen evolution reaction.

*Project supported by the National Basic Research Program, China (Grant Nos. 2016YFA0202300 and 2016YFA0202302), the National Natural Science Foundation of China (Grant Nos. 61527817, 61335006, and 61378073), and the Beijing Municipal Science and Technology Committee, China (Grant No. Z151100003315006).

†Corresponding author. E-mail: 983682235@qq.com

‡Corresponding author. E-mail: dwhe@bjtu.edu.cn

§Corresponding author. E-mail: yshwang@bjtu.edu.cn

© 2018 Chinese Physical Society and IOP Publishing Ltd

2. Materials and methods

2.1. Materials

Sulfuric acid (H_2SO_4), chloroauric acid ($HAuCl_4{\cdot}4H_2O$), sodium citrate, L-cysteine, sodium molybdate (Na_2MoO_4), and other reagents were purchased from Alfa Aesar. Deionized water was used for preparing all solutions.

2.2. Instrumentation

The morphologies of catalysts were characterized using field emission scanning electron microscopy (SEM) with an accelerating voltage of 15 kV (Hitachi S-4800, Japan). Transmission electron microscopy (TEM) images were achieved by a JEM-1400 operating at 120 kV. The x-ray photoelectron spectroscopy (XPS) measurement was carried on PHI Quantera (PHI, Japan), and the binding energy is calibrated with C 1s = 284.8 eV.

2.3. Electrochemical measurements

All electrochemical measurements were performed on a glass carbon electrode (GCE)by using a three-electrode CHI660D electrochemical workstation (Chenhua Instrument, Shanghai, China) in 0.5-M H_2SO_4 solution, platinum wire was used as a counter electrode, and a Ag/AgCl electrode served as a reference electrode. Typically, 6-μL AuNPs, MoS_2, and Au–MoS_2 composite inks were drop-casted onto the conventionally pretreated 3-mm-diameter GCEas working electrodes. In this study, all the potentials measured were verified by the reversible hydrogen electrode (RHE) according to the equation: $E_{\mathrm{RHE}} = E_{\mathrm{Ag/AgCl}} + 0.197 + 0.059$ pH. Linear sweep voltammetry (LSV) were swept from -0.8 V to 0.4 V versus RHE was swept with a scan rate of 0.05 V/s. The current density was calculated based on the geometric area of the GCE to be 7.07×10^{-2} cm^2.

2.4. Synthesis of MoS_2 and AuNPs

In a typical synthesis of the MoS_2, 0.2-g Na_2MoO_4 and 0.4-g L-cysteine were dissolved in 40-mL deionized (DI) water. The mixture was sonicated for 15 min. The homogeneous solution was then transferred into a 100-mL Teflon-lined stainless steel autoclave reactor, and hydrothermally treated in an oven at 180 °C for 12 h. The autoclave was then removed from the oven and naturally cooled to room temperature. The black product formed in the solution was then collected by centrifugation, washed with DI water and ethanol repeatedly many times, and then dried by lyophilization. Finally, the dried black product was dispersed in DI water with a concentration of 8 mg/mL.

Au nanoparticles were synthesized according to our previously reported method.[38] Briefly, 500-μL $HAuCl_4$ (25.4 mM) was added into 40-mL boiling distilled water under vigorous stirring, and 900-μL trisodium citrate (0.1 M) was dropwise added into the boiling solution under constant stirring for 20 min, the color changed to wine red when the reaction was completed. Finally, the suspension was cooled down to room temperature under continuous stirring and stored at 4 °C.

2.5. Fabrication of Au–MoS_2 composite

Au nanoparticles (NPs) were *in situ* synthesised on the MoS_2 nanoflower. Briefly, 0.75-mL MoS_2 aqueous solution was added into 20-mL DI water followed by the addition of $HAuCl_4$ (25.4 mM). $HAuCl_4$ solution volumes were set to be 10, 25, 50, 100, and 150 μL. The mixture was sonicated for 15 min. Then, the solution was heated to boiling under vigorous stirring, and excess trisodium citrate (0.1 M) was dropwise added into the mixture under constant stirring for another 20 min. After the suspension was cooled down to room temperature, the products were centrifugally washed with DI water four times. Finally, the black products were dispersed in 20-mL DI water. The composites were denoted as Au–MoS_2-10, Au–MoS_2-25, Au–MoS_2-50, Au–MoS_2-100, and Au–MoS_2-150, respectively.

3. Results and discussion

3.1. Morphologies and structures of MoS_2 and Au–MoS_2 composites

Figure 1 shows TEM images of MoS_2, Au–MoS_2-10, Au–MoS_2-25, Au–MoS_2-50, Au–MoS_2-100, Au–MoS_2-150, SAED pattern, and high-resolution TEM image of Au–MoS_2-100 composite. Few small dark spots were found to adhere to the surface as a consequence of Au loading and not observed outside the supporter. Distinct lattice fringes of Au and MoS_2 can be observed in the high-resolution TEM images with the fringe spaces of 0.18 nm and 0.64 nm, confirming that the (111) plane of AuNPs and the (002) plane of MoS2 exist respectively, which indicates the formation of Au–MoS_2 composites.[6,20] The AuNPs prepared by sodium citrate reduction have good monodispersity and an average diameter of 10 nm. The morphologies and crystal structures of MoS_2 and Au–MoS_2 composites were also studied by SEM (Fig. 2). MoS_2 exhibits the sphere-like aggregate morphology and the spheres are composed of thin nanosheets. The thin nanosheet will increase the specific surface area of MoS_2 and introduce more active sites, which is significantly important for the electrocatalytic activity of MoS_2. With the different volumes (10 μL–150 μL) of $HAuCl_4$ added into MoS_2 solution, the amount of AuNPs grown on the surface of the MoS_2 nanosheet increases. The right amount of AuNPs may improve the electronic property of MoS_2, but excess AuNPs can influence the active site on the MoS_2 nanosheets then reduce the catalytic performance of the system.

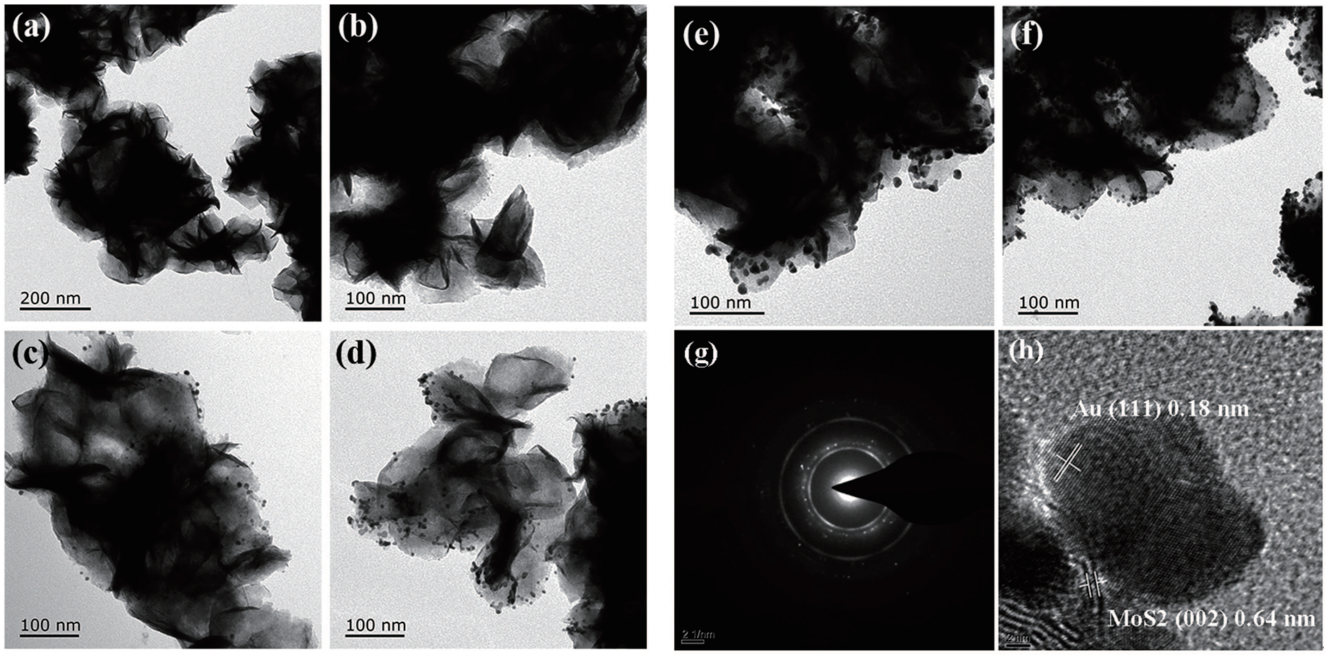


Fig. 1. TEM images of (a) pure MoS_2, (b) Au–MoS_2-10, (c) Au–MoS_2-25, (d) Au–MoS_2-50, (e) Au–MoS_2-100, and (f) Au–MoS_2-150. (g) SAED patterns of Au–MoS_2-100. (h) High-resolution TEM of AuNPs/$MosS_2$.

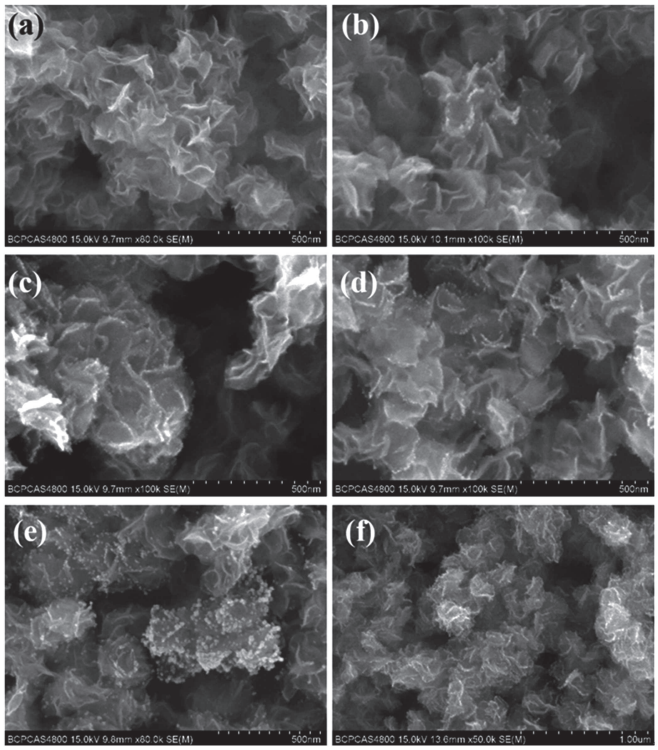


Fig. 2. SEM images of (a) pure MoS_2, (b) Au–MoS_2-10, (c) Au–MoS_2-25, (d) Au–MoS_2-50, (e) Au–MoS_2-100, and (f) Au–MoS_2-150.

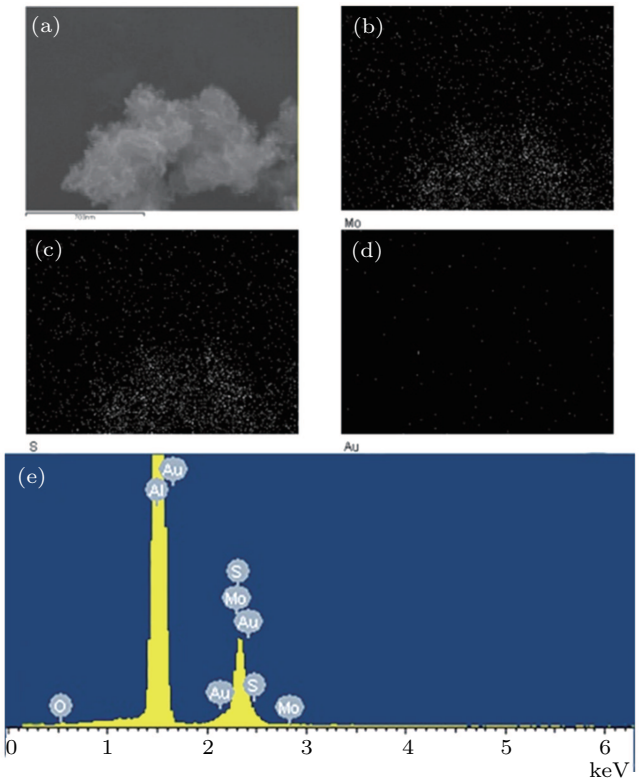


Fig. 3. (color online) EDS elemental mapping images of (a) Au–MoS_2-100 composite, (b) Mo, (c) S, (d) Au, and (e) energy dispersive x-ray spectrum of Au–MoS_2-100 composite.

The elemental mapping images based on Fig. 3(a) are displayed in Figs. 3(b)–3(d), demonstrating that Mo, S, and Au are uniformly distributed all over the nanosheets. Moreover, energy dispersive x-ray spectrum (Fig. 3(e)) shows that the as-synthesized Au–MoS_2 composite sample is mainly composed of Mo, S, and Au elements, indicating the successful synthesis of Au–MoS_2 composite.

To explore the composition and chemical bonding configuration, XPS spectra of MoS_2 are recorded before and after the introduction of Au. The XPS survey spectra of samples are shown in Fig. 4, which confirm the presence of Mo, S, and Au elements, no impurity phase is found. Two characteristic peaks at 227.1 eV and 230.4 eV are typical values for Mo

$3d_{5/2}$ and Mo $3d_{3/2}$ orbits (Fig. 4(b)) respectively, suggesting the dominance of the +4 oxidation state of the Mo element in MoS_2. The peaks at around 160.1 eV and 161.1 eV (Fig. 4(c)) are attributed to the coexistence of S $2p_{3/2}$ and $2p_{1/2}$ respectively, suggesting the −2 reduction state for the S element. The characteristic peak at 224.4 eV is related to S 2s. Detailed compositional analysis results reveal that the atomic ratio of Mo:S is about 1:2.11.[39] The peaks at 227.3 eV, 230.4 eV (Fig. 4(d)) and 160.2 eV, 161.3 eV (Fig. 4(e)) are all close to the binding energies of pure MoS_2 (Figs. 4(b) and 4(c)). This indicates that a similar chemical environment for the two elements in pure MoS_2 and Au–MoS_2 composite and the small binding energy shift may be caused by the electron transfer between AuNPs and MoS_2 sheets. The Au 4f peaks at 82.6 eV and 86.4 eV (Fig. 4(f)) can be detected, which indicates the successful synthesis of Au–MoS_2 composite.

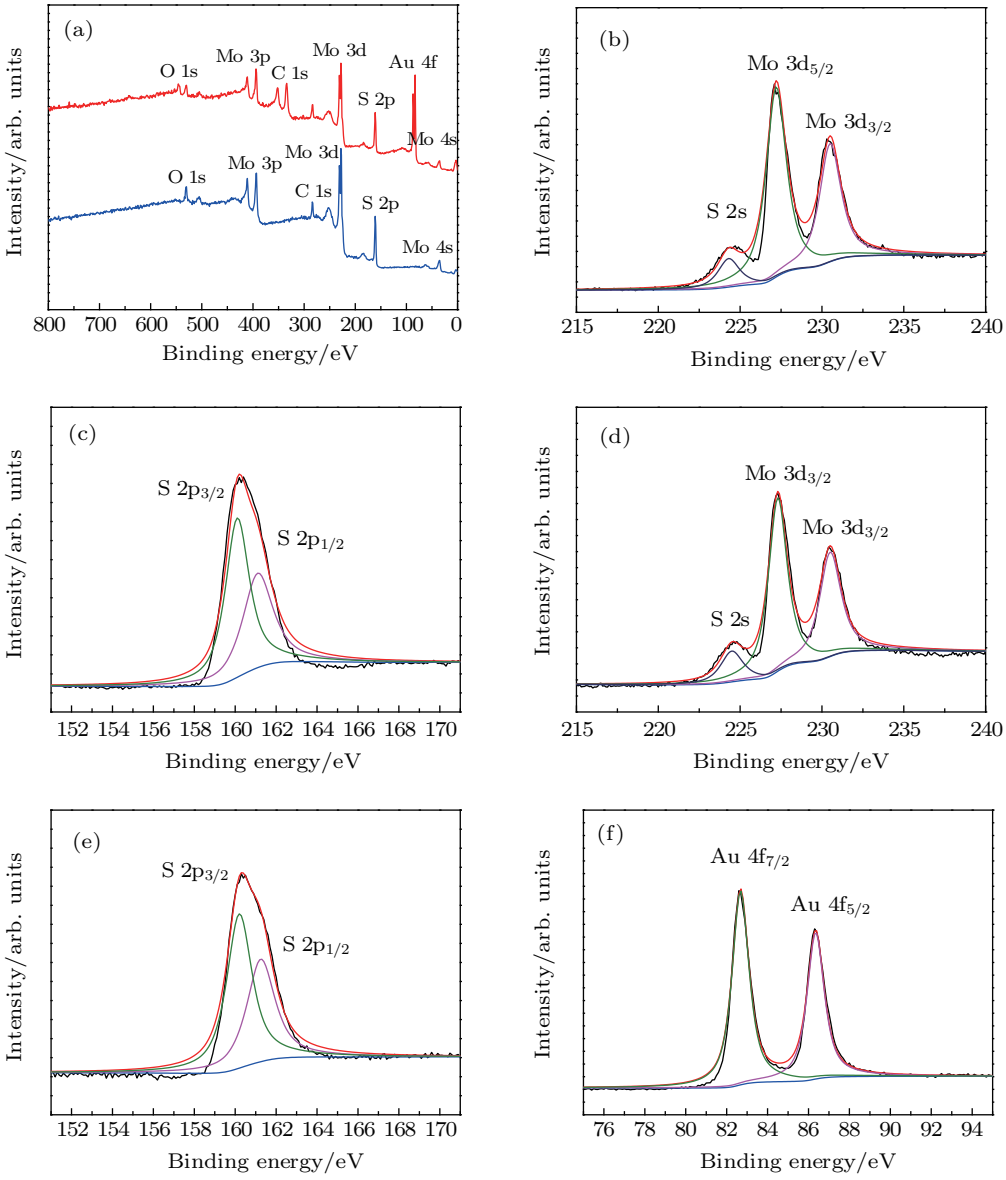


Fig. 4. (color online) (a) XPS survey spectra of pure MoS_2 and Au–MoS_2-100 composite. High-resolution XPS survey spectra of (b) Mo 3d and (c) S 2p. High-resolution XPS survey spectra of (d) Mo 3d, (e) S 2p, and (f) Au 4f.

3.2. Evolution of electrocatalytic activity

In order to evaluate the electrocatalytic HER activities of the Au–MoS_2 composites, glassy carbon electrodes modified with pure MoS_2, Au–MoS_2-10, Au–MoS_2-25, Au–MoS_2-50, Au–MoS_2-100, and Au–MoS_2-150 compositions are prepared for polarization curves in 0.5-M H_2SO_4 electrolyte. As shown in Fig. 5(a), the pure MoS_2 has a high onset overpotential of 300 mV, while all the Au–MoS_2 composites have a lower onset overpotential between 120 mV and 270 mV. The enhanced HER activity can be mainly attributed to the introduction of AuNPs, which improves electron transfer between electrode and MoS_2. The onset overpotential decreases with the increase of AuNPs, and Au–MoS_2-100 has the lowest onset overpotential of 120 mV, but when the concentration of AuNPs increases to Au–MoS_2-150, the overpotential reaches to 180 mV. This is most probably because too many AuNPs have grown on the

surface of MoS_2, thereby reducing the active sites on the edge nanosheets. That is, Au–MoS_2-100 has the best HER catalytic activity, which is better than Au–MoS_2-10 (270 mV), Au–MoS_2-25 (240 mV), Au–MoS_2-50 (230 mV), and Au–MoS_2-150 (180 mV).

The Tafel slope is an intrinsic nature of the electrocatalyst material. The Tafel slope derived from the polarization curves is shown in Fig. 5(b). The Au–MoS_2-10, Au–MoS_2-25, Au–MoS_2-50, Au–MoS_2-100, and Au–MoS_2-150 compositions are found to show Tafel slopes of 289 mV·dec^{-1}, 287 mV·dec^{-1}, 239 mV·dec^{-1}, 163 mV·dec^{-1}, and 284 mV·dec^{-1}, respectively. The smaller Tafel slope signifies a faster increase of HER rate with increasing overpotential. Therefore, the Au–MoS_2-100 has the smallest Tafel slope, supporting its best electrocatalystic activity for HER. Furthermore, electrochemical impedance spectroscopy (EIS) is used to study the interfacial reactions of the obtained samples under HER process. The EIS measurements are carried out in 0.5-M H_2SO_4 at an overpotential of 0.25 V. As shown in Fig. 5(c), the reaction resistance of Au–MoS_2 composite increases in the sequence of Au–MoS_2-150 <Au–MoS_2-100<Au–MoS_2-50<Au–MoS_2-25<Au–MoS_2-10, which is similar to the above HER results. The reaction resistances are 95 Ω for Au–MoS_2-150 and 177 Ω for Au–MoS_2-100, respectively, which are much smaller than those of Au–MoS_2-10 (360 Ω), Au–MoS_2-25 (270 Ω), and Au–MoS_2-50 (260 Ω), indicating that the AuNPs grown on MoS_2 can improve the conductivity and ensure high-quality catalytic activity in the HER process. Finally, the stability of the Au–MoS_2-100 catalytic response is also evaluated by conducting the cyclic voltammetry (CV). As can be seen from Fig. 5(d), after 200-CV cycles, the catalyst affords similar curves to the initial cycle with slight anodic current loss at a certain overpotential. These results indicate that the Au–MoS_2-100 has good stability in a long-term electrochemical process and has a promising potential for practical applications.

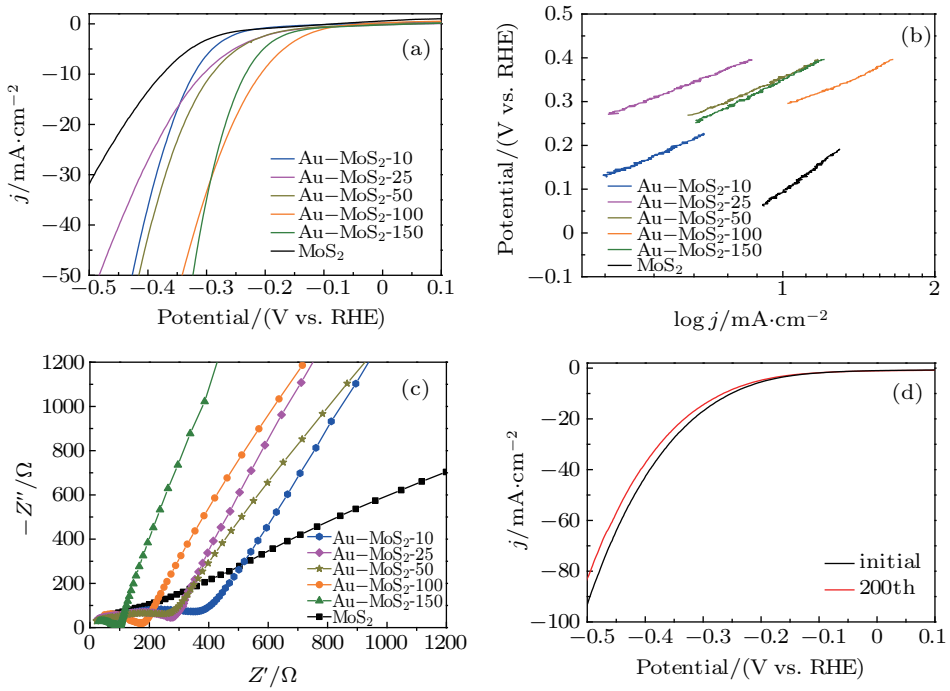


Fig. 5. (color online) (a) LSV curves for pure MoS_2, Au–MoS_2-10, Au–MoS_2-25, Au–MoS_2-50, Au–MoS_2-100, and Au–MoS_2-150. Corresponding (b) Tafel plots and (c) Nyquist plots. (d) LSV curves of the Au–MoS_2-100 at initial and 200 cycles for durability test.

4. Conclusions

Composites of Au–MoS_2 have been prepared by a solvothermal method. Au nanoparticles are *in situ* grown on the surface of a MoS_2 nanoflower. The hydrogen evolution activity of the composite can be adjusted by the number of AuNPs. The Au–MoS_2-100 shows excellent catalytic activity for hydrogen production with a lowest onset overpotential of 120 mV and a smallest Tafel slope of 163 mV·dec^{-1}. The outstanding performance of the Au–MoS_2-100 catalyst should be ascribed to the large specific surface area, large number of active sites, as well as more excellent ability to transfer electrons. Thus, the Au–MoS_2 composite is a good candidate for advanced HER electrocatalyst in practical applications.

References

[1] Zhang Y, Yan J, Ren X, Pang L, Chen H and Liu S 2017 *International Journal of Hydrogen Energy* **42** 5472
[2] Jin J, Zhu Y, Liu Y, Li Y, Peng W, Zhang G, Zhang F and Fan X 2017 *International Journal of Hydrogen Energy* **42** 3947
[3] Mo Q, Yao Y, Liu B, Peng L, Yan H, Hou Z, Wang J and Lin Y 2017 *Mater. Chem. Phys.* **193** 298
[4] Yang L, Zhu X, Xiong S, Wu X, Shan Y and Chu PK 2016 *ACS Appl. Mater. Interfaces* **8** 13966
[5] Zhang R, Li X, Zhang L, Lin S and Zhu H 2016 *Adv. Sci.* (Weinh) **3** 1600208

[6] Li A, Hu Y, Yu M, Liu X and Li M 2017 *International Journal of Hydrogen Energy* **42** 9419
[7] Xie J and Xie Y 2015 *ChemCatChem* **7** 2568
[8] Zhao X, Ma X, Sun J, Li D and Yang X 2016 *ACS Nano* **10** 2159
[9] Zhou H, Yu F, Sun J, He R, Wang Y, Guo CF, Wang F, Lan Y, Ren Z and Chen S 2016 *J. Mater. Chem. A* **4** 9472
[10] Li P, Yang Z, Shen J, Nie H, Cai Q, Li L, Ge M, Gu C, Chen X, Yang K, Zhang L, Chen Y and Huang S 2016 *ACS Appl. Mater. Interfaces* **8** 3543
[11] Pu Z, Liu Q, Asiri AM, Obaid AY and Sun X 2014 *Electrochimica Acta* **134** 8
[12] Zhang Q, Bai H, Zhang Q, Ma Q, Li Y, Wan C and Xi G 2016 *Nano Res.* **9** 3038
[13] Man Li Q M, Wei Zi, Xiaojing Liu, Xuejie Zhu and Shengzhong (Frank) Liu 2015 *Science Adv.* 1
[14] Xing Z, Liu Q, Asiri AM and Sun X 2014 *Adv. Mater.* **26** 5702
[15] Chen L, Yang W, Liu X and Jia J 2017 *International Journal of Hydrogen Energy* **42** 12246
[16] Khan M, Yousaf AB, Chen M, Wei C, Wu X, Huang N, Qi Z and Li L 2016 *Nano Res.* **9** 837
[17] Liu Y R, Li X, Han G Q, Dong B, Hu W H, Shang X, Chai Y M, Liu Y Q and Liu C G 2017 *International Journal of Hydrogen Energy* **42** 2054
[18] Dai X, Du K, Li Z, Liu M, Ma Y, Sun H, Zhang X and Yang Y 2015 *ACS Appl. Mater. Interfaces* **7** 27242
[19] Sun X, Dai J, Guo Y, Wu C, Hu F, Zhao J, Zeng X and Xie Y 2014 *Nanoscale* **6** 8359
[20] Yang J, Wang K, Zhu J, Zhang C and Liu T 2016 *ACS Appl. Mater. Interfaces* **8** 31702
[21] Guo B, Yu K, Li H, Song H, Zhang Y, Lei X, Fu H, Tan Y and Zhu Z 2016 *ACS Appl. Mater. Interfaces* **8** 5517
[22] Shen X, Xia X, Ye W, Du Y and Wang C 2016 *J. Solid State Electrochem.* **21** 409
[23] Xie J, Zhang H, Li S, Wang R, Sun X, Zhou M, Zhou J, Lou X W and Xie Y 2013 *Adv. Mater.* **25** 5807
[24] Deng J, Li H, Wang S, Ding D, Chen M, Liu C, Tian Z, Novoselov K S, Ma C, Deng D and Bao X 2017 *Nat. Commun.* **8** 14430
[25] Xiao Z, Song J, Ferry D K, Ducharme S and Hong X 2017 *Phys. Rev. Lett.* **118** 236801
[26] Chua X J and Pumera M 2017 *Phys. Chem. Chem. Phys.* **19** 6610
[27] Kibsgaard J, Chen Z, Reinecke B N and Jaramillo T F 2012 *Nat. Mater.* **11** 963
[28] Li Y, Wang H, Xie L, Liang Y, Hong G and Dai H 2011 *J. Am. Chem. Soc.* **133** 7296
[29] Voiry D, Salehi M, Silva R, Fujita T, Chen M, Asefa T, Shenoy V B, Eda G and Chhowalla M 2013 *Nano Lett.* **13** 6222
[30] Berit Hinnemann P G M, Jacob Bonde, Kristina P Jφrgensen, Jane H Nielsen, Sebastian Horch, Ib Chorkendorff, and Jens K Nφrskov 2005 *J. Am. Chem. Soc.* **127** 5308
[31] Thomas F Jaramillo K P J, Jacob Bonde, Jane H. Nielsen, Sebastian Horch, Ib Chorkendorff 2007 *Science* **317** 100.
[32] Smith A J, Chang Y H, Raidongia K, Chen T Y, Li L J and Huang J 2014 *Adv. Energy Mater.* **4** 1400398
[33] Huang X, Zeng Z, Bao S, Wang M, Qi X, Fan Z and Zhang H 2013 *Mol. Theor.* **4** 1444
[34] Wu X, Guo S and Zhang J 2015 *Chem. Commun.* **51** 6318
[35] Lavie A, Yadgarov L, Houben L, Popovitz-Biro R, Shaul T E, Nagler A, Suchowski H and Tenne R 2017 *Nanotechnology* **28** 24LT03
[36] Chen Y, Peng W C and Li X Y 2017 *Nanotechnology* **28** 205603
[37] Xiao C, Liu J, Yang A, Zhao H, He Y, Li X and Yuan Z 2015 *Microchimica Acta* **182** 1501
[38] Zhao X, He D, Wang Y, Hu Y and Fu C 2016 *Chem. Phys. Lett.* **647** 165
[39] Li D, Xiao Z, Golgir H R, Jiang L, Singh V R, Keramatnejad K, Smith K E, Hong X, Jiang L, Silvain J F and Lu Y 2017 *Adv. Electron. Mater.* **3** 1600335